J. Min. Metall. Sect. B-Metall. 51 (1) B (2015) 25 - 32

Journal of Mining and Metallurgy, Section B: Metallurgy

DETAILED CHARACTERIZATION OF COMPLEX BANDING IN AIR-COOLED BAINITIC STEELS

L. Morales-Rivas[a], H. Roelofs[b], S. Hasler[b], C. Garcia-Mateo[a], F.G. Caballero[a]

[a] National Center for Metallurgical Research (CENIM-CSIC), Madrid, Spain
[b] R&D, Swiss Steel AG, Emmenweidstr. 90, CH-6020 Emmenbrücke, Switzerland

(Received 31 March 2014; accepted 28 October 2014)

Abstract

The presence of banding in a hot-rolled air-cooled bainitic steel has been thoroughly characterized. The banded microstructure was observed due to distinctive sensitivities to the etching agent. Microstructural and crystallographic studies by means of Scanning Electron Microscopy and Electron Backscatter Diffraction did not reveal any substantial differences between bands and matrix. However, solute segregation of some alloying elements was detected by Wavelength-Dispersive Spectroscopy, it being found that bands are enriched in Cr, Mo and Si and depleted in Mn. Finally, a set of theoretical calculations suggested that the solidification mode is responsible for such unusual partitioning behavior, which is beneficial in terms of the bainitic transformation.

Keywords: Microstructural banding, carbide-free bainite, EPMA, EBSD.

1. Introduction

Reducing the weight of car components has led to more filigree parts and the use of stronger materials. Conventional solutions with quench and tempered steels not always fulfil the needs concerning technical reliability, economics and environmental friendliness. Air-cooled TRIP-assisted bainitic steels are sometimes clearly better in balancing these aspects leading to a successful introduction into car components during the last decade of this type of microstructure. Avoiding the use of expensive alloying elements like Ni and Mo, steelmakers have focussed on Mn and Cr alloying concepts.

But it is a well known metallurgy fact that high concentrations of some of those alloying elements tend to segregate during solidification. In this sense, substitutional elements such as Mn, Cr and Si are more likely to stay in solution within the liquid than in delta ferrite (δ-ferrite), thus leading during subsequent cooling to enriched and depleted regions in those elements [1-3]. Further thermomechanical treatments, as hot rolling, will result in the formation of a microstructural banding, that is, alternate bands of different phases or microconstituents. This is the case of the alternate bands of pearlite in a ferritic matrix [1, 3, 4-7] or bands of martensite in a ferritic or bainitic matrix [2, 5, 8-10].

The presence of microstructural banding is not a desirable phenomenon, since it introduces a degree of uncontrolled anisotropy in the material, depending not only on the banding severity but also on the test/observation direction, i.e. longitudinal or transversal. In the case of martensitic bands, a decrease in toughness is common, the presence of the hard phase induces premature crack nucleation related to heterogeneous hardness distributions [9, 11, 12].

In this work, banding revealed in a hot-rolled air-cooled granular bainitic steel has been characterized. For this purpose, techniques as Scanning Electron Microscope (SEM), together with Electron Probe Micro - Analyzer - Wavelength - Dispersive Spectroscopy (EPMA - WDS) and Electron Backscatter Diffraction (EBSD), have been used to depict the differences in the matrix and the bands.

2. Experimental

The investigated steel grade has a chemical composition of 0.23 C - 0.97Si - 1.55Mn - 1.55Cr - 0.14Mo - 0.15S (wt. %) [13]. The steel was conventionally hot rolled to bars with a diameter of 40 mm, followed by air cooling, ~2 ºC/s. The alloy contains high Mn and Cr to increase hardenability in order to avoid ferrite-pearlite formation before bainitic transformation. The high level of S, 0.15 wt. %, together with the addition of Mn ensures the good machinability performance by means of sufficient MnS formation. Si is added to prevent coarse cementite precipitation during bainite formation, a

* *Corresponding author: lucia.morales@cenim.csic.es*

DOI:10.2298/JMMB140331008M

hard and brittle phase which is detrimental for toughness [14].

Microstructural observation was done on longitudinal samples after grinding and polishing following the standard procedures. The bainitic microstructure was revealed using a 2 % Nital etching solution and examined by means of Light Optical Microscopy (LOM) and SEM. Volume fraction of bands and martensite/austenite constituent (M/A) was metallographically measured following the standard E 562-11 [15] on LOM and SEM micrographs respectively.

The overall fraction of retained austenite (γ) was determined by means of quantitative X-Ray Diffraction (XRD) analysis. For this purpose, samples were polished using 1 μ diamond paste and then subjected to several cycles of etching and polishing to obtain an undeformed surface. They were then step-scanned in a Brucker-Axs D8 X-ray diffractometer using unfiltered Co Kα radiation. The scanning speed (2θ) was less than 0.3 degree/min. The machine was operated at 40 kV and 30 mA. The volume fraction of retained austenite was calculated from the integrated intensities of (111), (200), (220) and (311) austenite peaks, and those of (110), (200) and (211) for ferrite, the use of this number of peaks avoids possible bias due to crystallographic texture [16].

For the identification of phases and crystalline orientations, samples were finally polished using colloidal silica suspension, the subsequent EBSD analysis was performed by means of a detector coupled to a SEM assisted by INCA (Oxford Instruments) software, operating at 20 KV. The EBSD analysis was executed in two steps. First, a high magnification EBSD scanning with a step size of 0.06 μm, was performed in order to design both a post-processing stage and a subsequent filter that would allow a more accurate quantification of phase volume fraction by improving the data interpretation. In the second step, an optimized EBSD map at lower magnification with a step size of 0.24 μm was obtained to examine and to quantify both the austenite distribution and the bainitic ferrite effective grain size within bands and matrix. In the present context, the effective grain size is defined as the mean distance between the high angle boundaries (> 15º), i.e the feature controlling impact thoughness [17].

The amount of alloying elements within and between bands was obtained by means of EPMA, using a JEOL JXA 8900 M microprobe with a WDS, on colloidal silica polished sample. This latest polishing stage was important to ensure surface quality, preventing factors other than composition differences from affecting the measured X-Ray intensities.

All the necessary theoretical calculations were performed by means of Thermo-Calc [18], using the TCFE7 database [19].

3. Results and Discussion

After the described thermomechanical heat treatment and as expected from the applied cooling rate, the actual microstructure consists of granular bainite, i.e. semi-equiaxed structure, see Fig. 1, formed by a mixture of 67 % bainitic ferrite (BF) and 33 % M/A constituent, out of which 20 % is austenite, according to the XRD analysis.

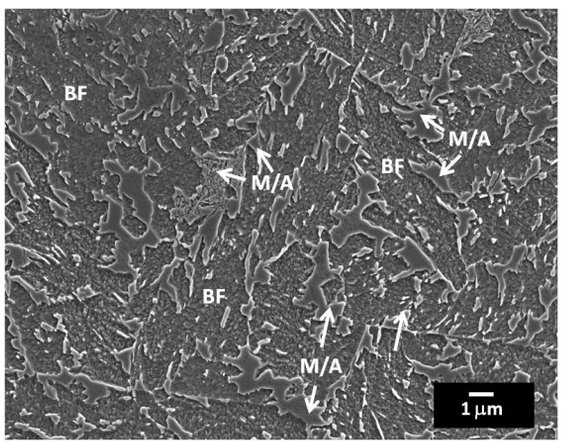

Figure 1. *Granular bainite formed by bainitic ferrite matrix (BF) and martensite/austenite (M/A) constituent revealed as non-etched islands and indicated by arrows.*

Fig. 2(a) illustrates an example of what in principle seems to be a typical severe banded structure. The volume fraction of bands, calculated using LOM micrographs of the type shown in Fig. 2(a), was 0.19±0.06. Higher magnifications, Fig. 2(b) are necessary to realize that there is not an apparent difference in microstructure within and between bands, it being bainitic ferrite and M/A constituent in both cases. Nonetheless, the resistance to etching is obviously different.

EBSD analyses were performed with the aim of finding out if more subtle differences in the microstructure were responsible for the heterogeneous etching resistance. As explained, a first scan at high magnification was performed as a way to obtain the best parameters in for a post-processing stage and the subsequent filter to remove the misindexed data. The INCA settings found to be the most suitable for the post-filtering are: high accuracy scanning, 7 minimum indexed bands and two phases to be indexed (Fe-α and Fe–γ). Then, the following filters were applied to remove non-reliable EBSD data (pixels randomly oriented and, thus, erroneously indexed): Pattern Quality Threshold (PQT) = 95 and 25, and Maximum Residual Angle (MRA) = 2.2 and 3, for the austenite orientation map and the ferrite orientation map, respectively. Then, for phase

identification, the filtered EBSD map was compared to a SEM micrograph of the same area, Fig. 3(a)-(d). To ease the observation, Fig 3(b) shows a drawing of Fig 3(a) (the revealed microstructure), where M/A constituent is colored as gray. The EBSD pattern quality map, Fig. 3(c), together with Fig. 3(b), indicate the poor quality of data belonging to M/A features, as it is expected, due to the high deformation associated to this microconstituent. Fig. 3(d) shows the phase map built after filtering ferrite and austenite separately, where yellow is for ferrite; pink, for austenite; and black, for unindexed pixels. The suitability of the process is confirmed by comparing Fig. 3(b) and Fig. 3(d), since it is possible to identify the phases and quantify its volume fraction by means of filtered EBSD maps, otherwise not possible: yellow pixels indicate the presence of ferrite, whereas pink plus black, the presence of M/A.

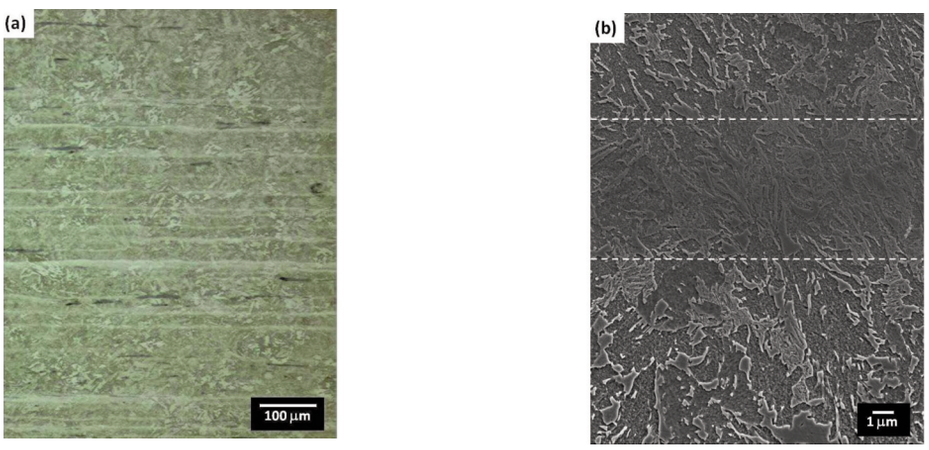

Figure 2. *(a) LOM and (b) secondary-electron SEM micrographs of a longitudinal sample after standard etching, revealing the presence of bands in a bainitic matrix. Dashed lines in the SEM micrograph delimit band region.*

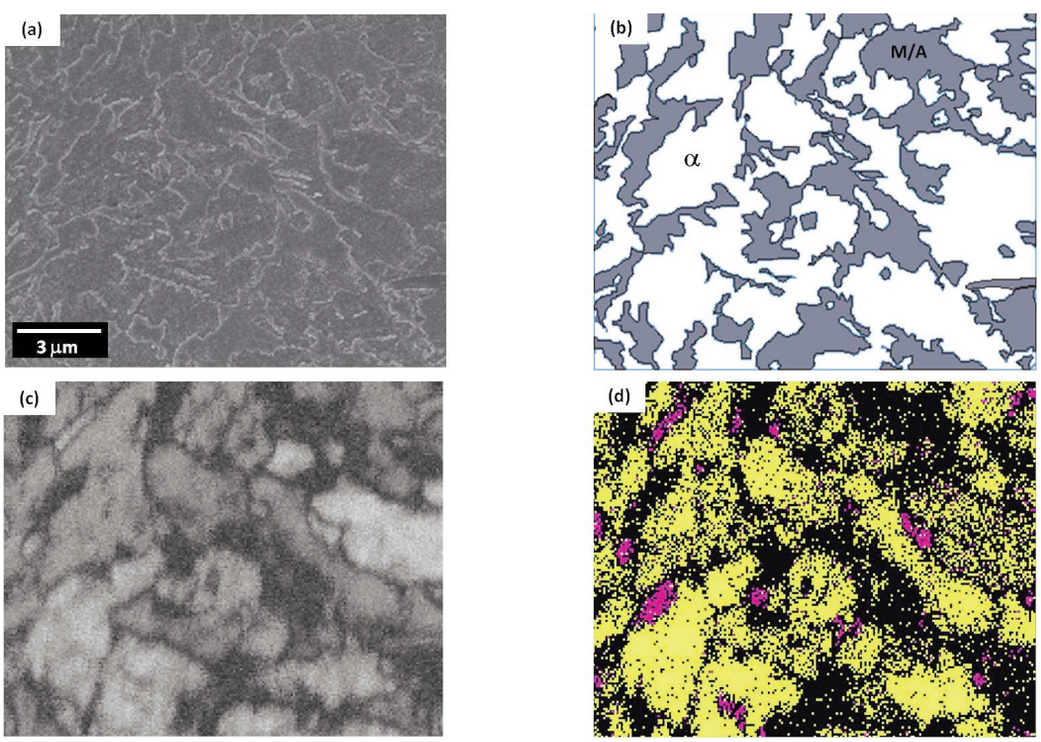

Figure 3. *The four pictures represent the same area, scanned by EBSD at high magnification: (a) Secondary Electron SEM micrograph after standard etching, revealing the microstructure; (b) drawing where gray features represent M/A constituent revealed in (a); (c) pattern quality map of EBSD scan; (d) phase map of EBSD scan, where yellow stands for ferrite, pink, for austenite and black for unindexed pixels.*

In the second stage of the EBSD analysis, scanning is done at lower magnification over an area including both matrix and band, Fig. 4(a); and the post-process and filter as explained above are applied, Fig. 4(b). The phase quantification performed in such fashion on Fig. 4(b) resulted in a M/A volume fraction in band of 50 % as compared with 40% in matrix.

Finally a set of measurements of the bainitic ferrite effective grain, delimited by high angle boundaries (>15º), were done on ferrite orientation map [20, 21]. Its distribution is shown in Fig. 5, and there is no evidence of differences in the effective grain size in and between bands.

From the point of view of the microstructure characterization, it can be concluded that the differences between the matrix and the band are restricted just to small variations of the phase volume fraction, but not to the phases themselves. A further step was taken, and the possibility of chemical segregation associated to bands and matrix was explored as a plausible explanation for the different etching resistance observed. For this purpose, the area shown in Fig. 6 was analyzed by EPMA, and results thus obtained revealed that there are diverse concentrations in some substitutional alloying elements. Qualitative maps corresponding to Si, Mn, S, Cr and Mo are presented in Fig. 7. It is evident that bands are enriched in Cr, Si and Mo and depleted in Mn when compared to the matrix. MnS inclusions are easily identified observing the corresponding element maps, Fig. 7.

Although maps are qualitative, following ref. [22] it is possible to estimate contents in the different alloying elements in bands and matrix, excluding inclusions. Thus, the signal intensity detected for every element is assumed to be directly dependant on its wt. %, having recorded maps large enough to be representative of the whole microstructure, so that the average wt. % of each element is equal to the bulk. In fact, the volume fraction of bands in the scanned area, in Fig. 6 and Fig.7, is equal to that calculated using LOM micrographs, ~0.19.

In the case of Mn, the calculation of the amount in solid solution (s.s.) is estimated by considering that all

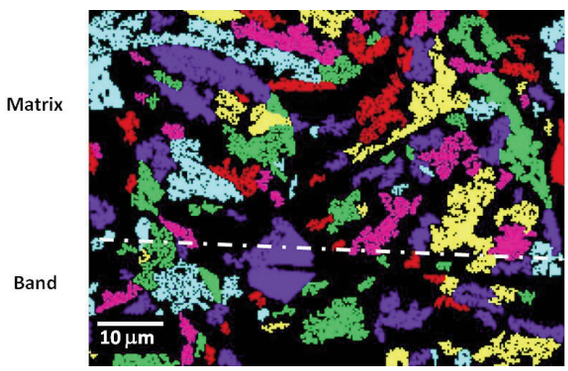

Figure 5. *Grain map of ferrite from Figure 5 delimited by high angle boundaries (>15º), grains are identified by different colours.*

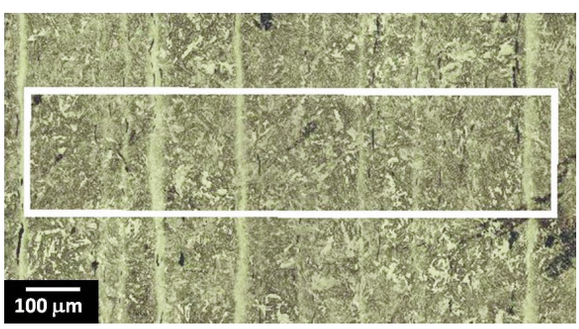

Figure 6. *LOM micrograph of the revealed microstructure showing the area scanned by EPMA (white rectangle). Bands lay vertically.*

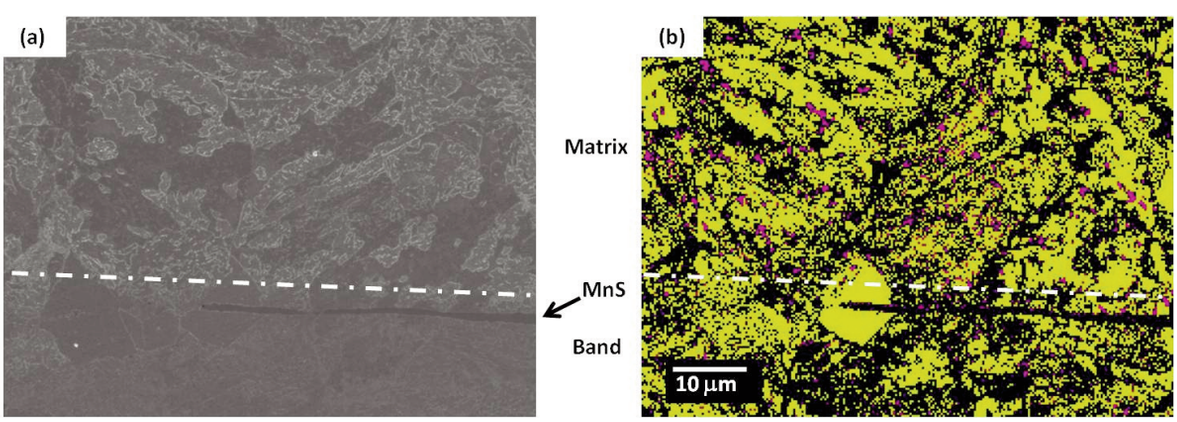

Figure 4. *(a) Phase map of a low magnification EBSD map and (b) the SEM micrograph of the same area, after etching, revealing the presence of a band, below the dotted line. In the phase map, yellow stands for ferrite; pink, for austenite and black, for unindexed pixels. It is also noticeable the presence of a MnS inclusion, which has not been indexed.*

the S is tied up as MnS, which is consistent with theoretical calculations [19]. Thus, the total amount of Mn that remains in s.s. is 1.29 wt. %. Finally, in Table 1, the estimated contents of the different alloying elements in bands and matrix are presented, confirming what it was anticipated in Fig. 7, i.e. bands are enriched in Cr, Si and Mo and depleted in Mn.

Table 1. *Chemical composition in wt. % of bands and matrix, estimated according to EPMA results.*

Region / Element	Band	Matrix
Cr	1.82	1.45
Si	1.11	0.92
Mo	0.17	0.13
Mn	1.18	1.3

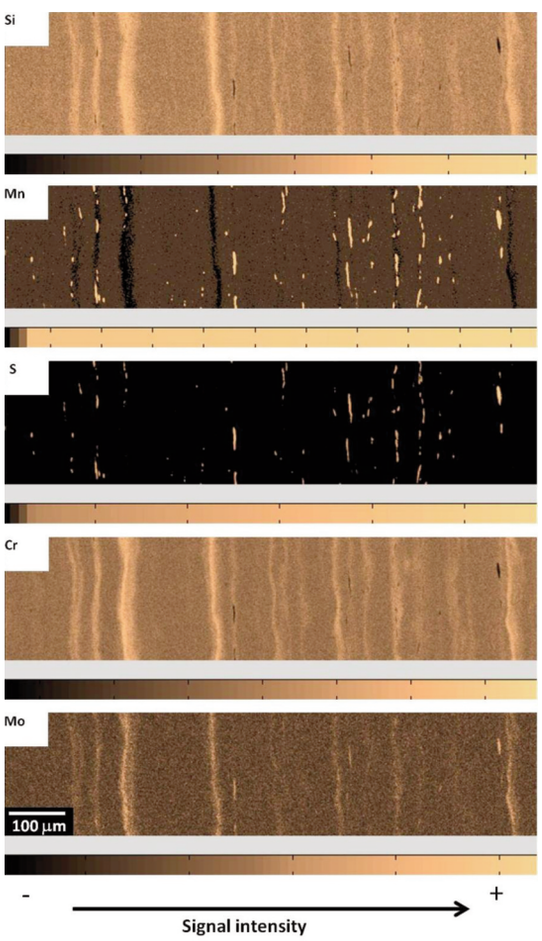

Figure 7. *EPMA maps showing the signal intensity detected for every alloying element (Cr, Si, Mo, Mn and S), which is proportional to their weight %. Most inclusions are found to be MnS. The color scale for each map has been properly changed to improve the image contrast.*

These results were rationalized using theoretical calculations on the phase evolution during solidification by means of Thermo-Calc [19]. The diagram in Fig. 8 reveals a solidification path that starts with the formation of δ-ferrite from the liquid (L) and ends with the peritectic solidification of austenite phase (γ) from L and δ-ferrite. Table 2 shows the theoretical partition coefficients, concentration ratios between the liquid and the two solid phases, K(δ/L) and K(γ/L), derived from calculations [19] at the temperature of interest where the 3 phases co-exist. The coefficients imply the same "direction" of partitioning, that is, they are < 1, meaning that all substitutional alloying elements present a trend to partition from δ-ferrite and from γ into the liquid, making the latter enriched in those elements. This fact does not match the EPMA results, suggesting that Mn segregates the opposite way than the other alloying elements.

Table 2. *Partition coefficients between δ-ferrite and liquid (L), and between austenite (γ) and L, from Thermo-Calc, at the temperature where δ-ferrite, L and γ coexist.*

	K(δ/L)	K(γ/L)
Cr	0.91	0.9
Si	0.69	0.66
Mo	0.67	0.49
Mn	0.62	0.69

On the other hand, MnS inclusions may be playing an important role. Because the liquid gets richer in Mn and S as solidification takes place, MnS is very prone to precipitate in that state. The consequent decrease in the Mn content in the liquid has been reported to be the reason of the banded region [2, 23]. But, after a detailed examination to assess the distribution of inclusions within and between bands, using micrographs like this shown in Fig. 9, there is no evidence of preferential precipitation of inclusions within the bands or in the matrix, they are homogeneously distributed. Only minute quantities of pro-eutectoid ferrite are found to be associated to MnS in both bands (Fig. 4) and matrix (Fig. 10), which is consistent with local Mn depletion nearby the inclusion. Therefore it is difficult to explain the overall Mn depletion in bands by this mechanism.

Another explanation for the chemical segregation is the solute partition between δ-ferrite and γ. This is evaluated in Table 3, where it can be seen that the calculated partition coefficients in equilibrium at the temperature where the 2 phases co-exist, K(γ/δ), shows that all elements but Mn have coefficients below 1, implying, in this case, different partitioning "directions". The concentration ratios calculated from EPMA results between matrix and band, K(M/B) in

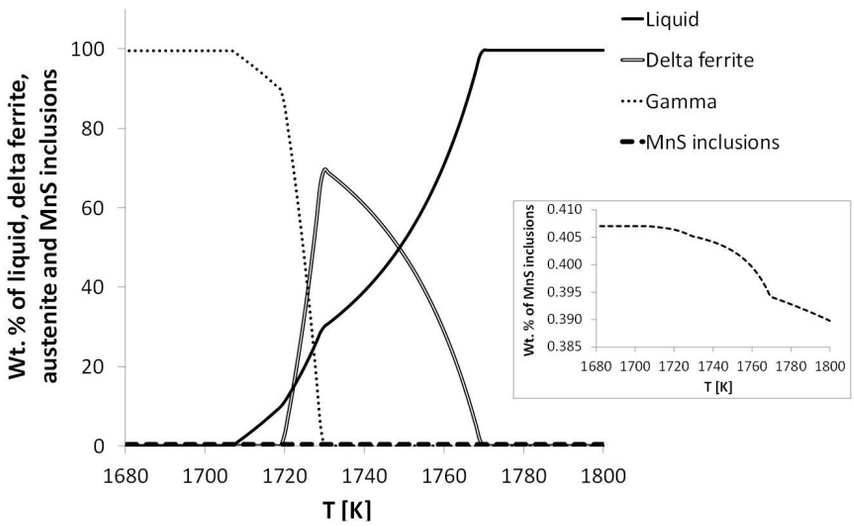

Figure 8. *Phase evolution during solidification, according to equilibrium conditions, and an enlarge detail of the MnS field.*

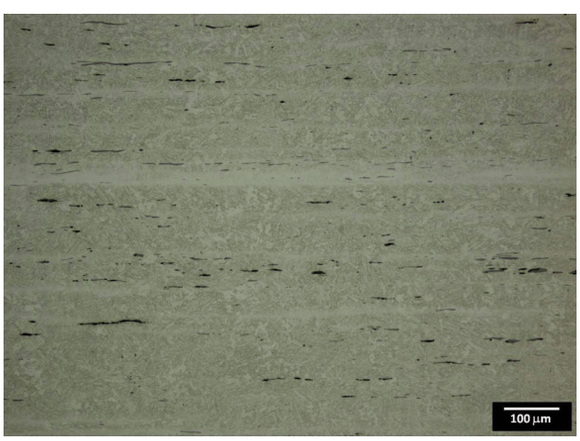

Figure 9. *Optical micrograph showing the banded microstructure and the presence of MnS inclusions.*

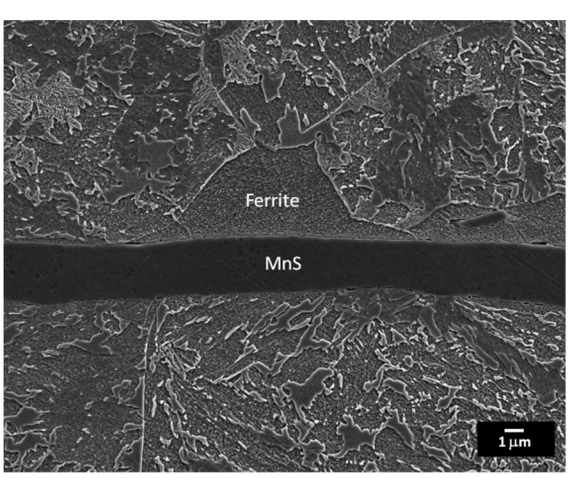

Figure 10. *Proeutectoid ferrite (plain grey grain) associated to a MnS inclusion (black elongated feature).*

Table 3, show an excellent agreement with those theoretically calculated, K(γ/δ). This behavior could be explained if we keep in mind that the peritectic solidification, L+δ→L+δ+γ, actually occurs in two steps: first, the so-called peritectic reaction, in which L reacts with δ-ferrite resulting in the formation of γ along their interface; and second, when there is a complete layer of γ acting as a barrier between L and δ, the growth of γ phase continues throughout the peritectic transformation, split into two single reactions, L→γ and δ-ferrite→γ [24, 25]. The rate of the thickening of γ phase toward L is likely to be faster than toward δ phase [25, 26]; therefore, once the entire amount of L has transformed into γ, the only reaction taking place is δ-ferrite→γ. Thus, the complete solidification path in our case could be the same as the well known *FA mode* of austenitic stainless steels: L→L+δ→ L+δ+γ →δ+γ→γ [27, 28].

Table 3. *Partition coefficients between γ and δ-ferrite, from Thermo-Calc, at the temperature where δ-ferrite, L and γ coexist, and concentration ratios between matrix and band, from EPMA analysis.*

	K(γ/δ)	K(M/B)
Cr	0.98	0.8
Si	0.96	0.82
Mo	0.73	0.76
Mn	1.11	1.1

There is evidence that shows that δ→γ transformation may occur under partitioning local equilibrium or under paraequilibrium (only C diffuses) depending on the chemical composition and/or temperature [24, 25, 28-31]. Attending to this and on the basis of our experimental results, we can

speculate that at high temperatures during the first stage of δ→γ transformation, the substitutional alloying elements are allowed to diffuse and segregate according to their alphagenic or gammagenic nature [25, 27-30]. At lower temperatures, the diffusion of substitutional elements is negligible and δ→γ transformation may take place close to the paraequilibrium conditions. Even if δ→γ is not completed, the subsequent thermomechanical process would enhance the transformation of the remaining δ-ferrite into γ under conditions near paraequilibrium [32]. Therefore, the substitutional alloying content of δ-ferrite, according to the chemical segregation during the first stage of the δ→γ transformation, can be inherited by the product γ at the second stage, resulting in the final chemical banding observed.

Regardless of the solidification path that explains the substitutional element segregation found in this work, it is possible to theoretically justify the presence of the same final microstructure in both the matrix and the bands. As shown before, the whole microstructure is granular bainite, therefore the transformation took place between the B_s (bainite start temperature) and M_s (martensite start temperature). Thus, it is very unlikely that C has been segregated, unlike the case of slow cooling rates, where C can diffuse in accordance with the segregation of the substitutional elements that causes some regions to transform before others, resulting in the rejection of C to the areas that transform later [2, 33, 34]. Attending to bainite transformation theory [14], B_s is calculated as the temperature at which bainite nucleation and growth conditions are fulfilled, $\Delta G_m < G_N$ and $\Delta G^{\gamma\to\alpha} < -G_{SB}$, respectively. Where ΔG_m is the maximum free energy change accompanying the nucleation under paraequilibrium conditions; G_N, is the universal nucleation function and defines the minimum free energy change in order to nucleate bainite; $\Delta G^{\gamma\to\alpha}$ is the free energy change of the transformation of γ into α without any change in chemical composition [14]; and G_{SB} is the stored energy of the ferrite due to the displacive mechanism of transformation (400 J/mol) [14, 35-37]. In the same manner, M_s is calculated as the temperature at which the athermal, diffusionless nucleation and growth of martensite becomes possible, i.e., the condition $\Delta G^{\gamma\to\alpha} < G_N^{\alpha'}$ is fulfilled [38]. Results thus obtained are summarized in Table 4, and closely show that only small differences about 10º in the transformation temperatures, B_s and M_s, are found between the bands and the matrix, meaning that the lack of Mn in bands is balanced by the higher content in other elements, Cr, Mo, Si, and the other way around for the matrix.

Table 4. *B_s and M_s temperatures calculated for the chemical composition of matrix and of band.*

	B_s /ºC	M_s /ºC
Matrix	505	370
Band	495	365

4. Conclusions

In this work detailed microstructural characterization using Scanning Electron Microscopy, X-Ray diffraction and Electron Backscatter Diffraction failed to reveal any substantial differences that might explain the distinctive etching sensitivities observed in a banded bainitic steel. Only Electron Probe Microanalysis in conjunction with some theoretical calculations allowed to speculate that the observed banding is a direct consequence of the solidification path, where regions of the cast get depleted in Mn and enriched in Si, Cr and Mo. These differences explain the fact that the bainitic microstructure is the same in the bands and the matrix.

Acknowledgement

The authors would like to thank the Microscopy Center of the Polytechnic University of Valencia (UPV) and the ICTS National Centre for Electron Microscopy (CNME), located at the Complutense University of Madrid, for the EBSD and EPMA facilities, respectively. The authors would like to express their gratitude to Dr. D. San Martin for fruitful discussion and guidance on the solidification insights. LMR, CGM and FGC acknowledge the Spanish Ministry of Economy and Competitiveness (MINECO) for financial support in the form of a National Project MAT2010-15330 and an associated FPI grant.

References

[1] P.G. Bastien, J. Iron Steel Inst., 187 (1957) 281-291.

[2] H.K.D.H. Bhadeshia, Bulletin of the Polish Academy of Sciences, Technical Sciences, 58 (2010) 255-265.

[3] J.S. Kirkaldy, J. von Destinon-Forstmann, R.J. Brigham, Can. Metall. Quart., 59 (1962) 59-81.

[4] A. Sakir Bor, ISIJ Int., 31 (1991) 1445-1446.

[5] F.G. Caballero, A. García-Junceda, C. Capdevila, C.G. De Andrés, Mater. Trans. JIM, 47 (2006) 2269-2276.

[6] J. Komenda, R. Sandström, Mater. Charact., 31 (1993) 143-153.

[7] P. Shanmugam, S.D. Pathak, Eng. Fract. Mech., 53 (1996) 991-1005.

[8] R.A. Grange, Metall. Trans. A, 2 (1971) 417-426.

[9] F.G. Caballero, J. Chao, J. Cornide, C. García-Mateo, M.J. Santofimia, C.Capdevila, Mater. Sci. Eng., A. 525 (2009) 87–95.

[10] Standard Practice for Assessing the Degree of Banding or Orientation of Microstructures, ASTM, E 1268-01 (2001).

[11] R.A. Jaramillo, M.T. Lusk, M.C. Mataya, Acta Mater.,

52 (2004) 851-858.

[12] C.R. Brooks, Banding in Steels, in C.R. Brooks (Ed.) Principles of the Austenitization of Steels, Elsevier Science, 1992, 40-50.

[13] H. Roelofs, U. Urlau, M. Lembke, G. Olschewski, 2nd Int Conf. On Steels in Cars and Trucks, Wiesbaden. (2008), 1-5.

[14] H.K.D.H. Bhadeshia, Bainite in Steels, Second ed., Institute of Materials, Maney Publishing, London, 2001.

[15] Standard Test Method for Determining Volume Fraction by Systematic Manual Point Count, E 562 – 11 (2011).

[16] M.J. Dickson, J. Appl. Crystallogr., 2 (1969) 176-180.

[17] F.G. Caballero, H. Roelofs, S. Hasler, C. Capdevila, J. Chao, J. Cornide, C. Garcia-Mateo, Mater. Sci. Technol, 28 (2012) 95-102.

[18] J.O. Andersson, T. Helander, L. Höglund, P.F. Shi, and B. Sundman, Thermo-Calc and DICTRA, Computational tools for materials science. Calphad, 26 (2002) 273-312.

[19] Thermo-Calc Software TCFE7 Steels/Fe-alloys database version 6.

[20] A.F. Gourgues, H.M. Flower, T.C. Lindley, Mater. Sci. Technol., 16 (2000) 26–40.

[21] J.M. Rodriguez-Ibabe, in: J.M. RodriguezIbabe, I. Gutierrez, B. Lopez (Eds.) Proceedings of the International Conference on Microalloying in Steels, 1998, p. 51-62.

[22] C. Celada, I. Toda-Caraballo, B. Kim, D. San Martín, Mater. Charact., 84 (2013) 142-252.

[23] J.S. Kirkaldy, R.J. Brigham, H.A. Domian, and R.G. Ward, Can. Metall. Quart., 2 (1963) 233–241.

[24] J.J. Ruiz Mondragon, M. Herrera Trejo, M.d.J. Castro Roman, H. Solis, ISIJ Int., 48 (2008) 454-460.

[25] Y.J. Choi, Non-equilibrium Solidification of δ-TRIP Steel, Master Thesis, Pohang University of Science and Technology (2011).

[26] Y. Aray, T. Emi, H. Fredriksson, H. Shibata, Metall. Mater. Trans. A, 36 (2005) 3065-3074.

[27] K. Rajasekhar, C.S. Harendranath, R. Raman, S.D. Kulkarni, Mater. Charact., 38 (1997) 53-65.

[28] J.W. Fu, Y.S. Yang, J.J. Guo, J.C. Ma, W.H. Tong, J. Cryst. Growth, 311 (2008) 132-136.

[29] T. Zhou, H.S. Zurob, E. Essadiqi, B. Voyzelle, Metall. Mater. Trans. B, 42A (2011) 3349-3357.

[30] T. Koseki, H. Inoue, H. Morimoto, S. Ohkita, Prediction of solidification and phase transformation of stainless steel weld metals, Nippon Steel Technical Report (1995) 33-40.

[31] H.L. Yi, S.K. Ghosh, W.J. Liu, K.Y. Lee, H.K.D.H. Bhadeshia, Mater. Sci. Technol., 26 (2010) 817-823.

[32] H.L. Yi, K.Y. Lee, H. Bhadeshia, Mater. Sci. Technol., 27 (2011) 525-529.

[33] D. Chahae, D.A. Koss, A.L. Wilson, P.R. Howell, Metall. Mater. Trans. A, 31A (2000) 995-1005.

[34] T.F. Majka, D.K. Matlock, G. Krauss, Metall. Mater. Trans. A, 33A (2002) 1627-1637.

[35] H. K. D. H. Bhadeshia: Acta Metall. 29 (1981) 1117.

[36] C. Garcia-Mateo, H. K. D. H. Bhadeshia: Mater. Sci. Eng. A. 378 (2004) 289.

[37] G. B. Olson, M. Cohen: Metall. Trans. A. 7 (1976) 1897.

[38] G. Ghosh, G. B. Olson: Acta Metall. Mater. 42 (1994) 3361.